ELSEVIER

International Journal of Solids and Structures 41 (2004) 637–662

INTERNATIONAL JOURNAL OF SOLIDS and STRUCTURES

www.elsevier.com/locate/ijsolstr

A simple spinning laminated composite shaft model

Min-Yung Chang *, Jeng-Keag Chen, Chih-Yung Chang

Department of Mechanical Engineering, National Chung Hsing University, 250 Kuo-Kuang Rd., Taichung, 402 Taiwan, ROC

Received 22 September 2003; received in revised form 22 September 2003

Abstract

A simple spinning composite shaft model is presented in this paper. The composite shaft contains discrete isotropic rigid disks and is supported by bearings that are modeled as springs and viscous dampers. Based on a first-order shear deformable beam theory, the strain energy of the shaft are found by adopting the three-dimensional constitutive relations of material with the help of the coordinates transformation, while the kinetic energy of the shaft system is obtained via utilizing the moving rotating coordinate systems adhered to the cross-sections of shaft. The extended Hamilton's principle is employed to derive the governing equations. In the model the transverse shear deformation, rotary inertia and gyroscopic effects, as well as the coupling effect due to the lamination of composite layers have been incorporated. To verify the present model, the critical speeds of composite shaft systems are compared with those available in the literature. A numerical example is also given to illustrate the frequencies, mode shapes, and transient response of a particular composite shaft system.

Keywords: Spinning shaft; Composite material; Critical speed

1. Introduction

The composite-material shafts have been sought as new potential candidates for replacement of the conventional metallic shafts in many application areas. This may be attributed to the improved performance of the shaft system resulting from the use of the composite materials. It was in fact demonstrated by Faust et al. (1984) via testing the composite transmission shafts of twin-propeller helicopters that the composite shaft not only is lighter in weight and has a lower vibration level, but also has greater strength and a longer service life compared with its metallic counterparts. Accompanied by the development of many new advanced composite materials, various mathematical models of spinning composite shafts were also developed by researchers. They include Zinberg and Symonds (1970) who used an equivalent modulus beam theory (EMBT) to model the composite shaft and compared the critical speeds with those of the tests

* Corresponding author. Tel.: +886-422840433; fax: +886-422877170.
E-mail address: minchang@dragon.nchu.edu.tw (M.-Y. Chang).

0020-7683/$ - see front matter © 2003 Elsevier Ltd. All rights reserved.
doi:10.1016/j.ijsolstr.2003.09.043

they had performed. dos Reis et al. (1987) incorporated the Timoshenko beam theory with the Donnell thin shell theory to derive the stiffness matrix of rotating composite shafts. They then adopted the approximate finite element approach of Ruhl and Booker (1972) to derive the equations of motion of systems. The model was used to analyze the critical speeds of thin-walled composite shafts.

Kim and Bert (1993) adopted a shell theory of first-order approximation to derive the governing equations of the rotating composite thin-walled shafts. They used this model to analyze the critical speeds of various types of composite shafts. Bert (1992) based on the Bernoulli–Euler theory developed the governing equations of composite shafts. The model has included the gyroscopic as well as the bending and torsion coupling effects. Bert and Kim (1995) further considered the Bresse–Timoshenko beam theory and employed the Hamilton's principle to derive the equations of motion of the composite shafts. They found that the transverse shear deformation effect is important in the determination of the critical speeds of the short shafts. Singh and Gupta (1996) presented two composite spinning shaft models based on an EMBT and a layerwise beam theory respectively. In the latter shaft model, the strain–displacement relations of the layerwise cylindrical shell theory considered by Alam and Asnani (1984) were adopted. They found that a discrepancy exists between the critical speeds obtained from these two models for the case of the unsymmetric laminated composite shaft, which they attributed to the effect of the bending and stretching deformation. Song et al. (2001) developed a composite thin-walled shaft model based on a thin-walled beam theory. This model was used to investigate the natural frequencies and stability of the system subject to the variation of the axial edge load and the lamination angle of the composite layer.

The shaft models being discussed above are mostly based on shell theories, or beam theories combined with the strain–displacement relations of the shell theories, or a thin-walled beam theory. In this paper, another simple composite shaft model based on a first-order beam theory is proposed. Here, however, the pertinent strain–displacement and the constitutive relations for laminated composite shafts are directly derived from those of three-dimensional continua through multiple coordinate transformations and the thinness of the wall of the shaft *is not* assumed. The composite shaft is assumed supported by bearings, which are modeled as springs and dampers, and has discrete isotropic rigid disks attached to it. The governing equations of system are obtained by employing the extended Hamilton's principle.

To determine the spinning shaft system's responses, the numerical finite element method is used here to approximate the governing equations by a system of ordinary differential equations. Based on these approximate equations the critical speeds of the spinning composite shaft systems are then analyzed. The results are found in agreement with those found in the literature. For a further illustration of the present shaft model, the frequencies, mode shapes, and the transient response caused by the unbalance force of a rigid disk, of a particular spinning composite shaft system are given. The transient response of the spinning shaft is obtained by using two independent procedures, the modal versus Newmark-β methods. The closeness of the results obtained from these two approaches does indicate the correctness of the numerical analyses performed in the paper.

2. Theoretical formulations

2.1. Composite shaft

Before apply the extended Hamilton's principle, firstly, the kinetic energy and strain energy of the laminated composite shaft will be derived. The constitutive relations for a lamina (see Fig. 1) in the principal material directions (indicated by 1, 2 and 3) are given by (see e.g., the monograph of Vinson and Sierakowski, 1986)

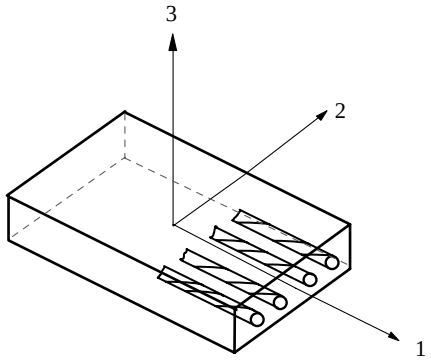

Fig. 1. A typical composite lamina and its principal material axes.

$$\begin{Bmatrix} \sigma_{11} \\ \sigma_{22} \\ \sigma_{33} \\ \tau_{23} \\ \tau_{31} \\ \tau_{12} \end{Bmatrix} = \begin{bmatrix} Q_{11} & Q_{12} & Q_{13} & 0 & 0 & 0 \\ Q_{12} & Q_{22} & Q_{23} & 0 & 0 & 0 \\ Q_{13} & Q_{23} & Q_{33} & 0 & 0 & 0 \\ 0 & 0 & 0 & Q_{44} & 0 & 0 \\ 0 & 0 & 0 & 0 & Q_{55} & 0 \\ 0 & 0 & 0 & 0 & 0 & Q_{66} \end{bmatrix} \begin{Bmatrix} \varepsilon_{11} \\ \varepsilon_{22} \\ \varepsilon_{33} \\ \gamma_{23} \\ \gamma_{31} \\ \gamma_{12} \end{Bmatrix} \tag{1}$$

The above equation will be abbreviated as

$$\{\sigma\} = [Q]\{\varepsilon\} \tag{2}$$

where $[Q]$ is the stiffness matrix. Consider an arbitrary layer of the laminate whose fiber direction makes an angle η with respect to the x-axis of the cylindrical coordinate system (x, r, θ) as shown in Fig. 2. Then the stress–strain relations of the components expressed in this chosen cylindrical coordinate system can be written as (Vinson and Sierakowski, 1986)

$$\begin{Bmatrix} \sigma_{xx} \\ \sigma_{\theta\theta} \\ \sigma_{rr} \\ \tau_{r\theta} \\ \tau_{xr} \\ \tau_{x\theta} \end{Bmatrix} = \begin{bmatrix} \overline{Q}_{11} & \overline{Q}_{12} & \overline{Q}_{13} & 0 & 0 & \overline{Q}_{16} \\ \overline{Q}_{12} & \overline{Q}_{22} & \overline{Q}_{23} & 0 & 0 & \overline{Q}_{26} \\ \overline{Q}_{13} & \overline{Q}_{23} & \overline{Q}_{33} & 0 & 0 & \overline{Q}_{36} \\ 0 & 0 & 0 & \overline{Q}_{44} & \overline{Q}_{45} & 0 \\ 0 & 0 & 0 & \overline{Q}_{45} & \overline{Q}_{55} & 0 \\ \overline{Q}_{16} & \overline{Q}_{26} & \overline{Q}_{36} & 0 & 0 & \overline{Q}_{66} \end{bmatrix} \begin{Bmatrix} \varepsilon_{xx} \\ \varepsilon_{\theta\theta} \\ \varepsilon_{rr} \\ \gamma_{r\theta} \\ \gamma_{xr} \\ \gamma_{x\theta} \end{Bmatrix} \tag{3}$$

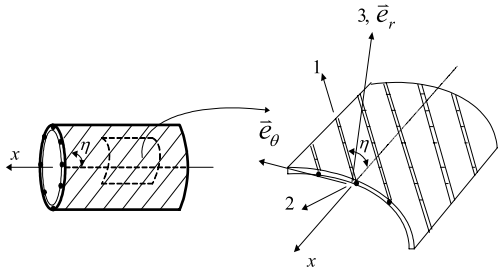

Fig. 2. The definitions of the principal material coordinate axes on an arbitrary layer of the composite shaft.

The above equation will be expressed in abbreviated form as

$$\{\sigma\} = [\overline{Q}]\{\varepsilon\} \tag{4}$$

where $[\overline{Q}]$ is the transformed stiffness matrix of the layer, and

$$[\overline{Q}] = [T]^{-1}[Q][T]^{-\mathrm{T}} \tag{5}$$

in which

$$[T] = \begin{bmatrix} m^2 & n^2 & 0 & 0 & 0 & 2mn \\ n^2 & m^2 & 0 & 0 & 0 & -2mn \\ 0 & 0 & 1 & 0 & 0 & 0 \\ 0 & 0 & 0 & m & -n & 0 \\ 0 & 0 & 0 & n & m & 0 \\ -mn & mn & 0 & 0 & 0 & (m^2 - n^2) \end{bmatrix} \tag{6}$$

and

$$m = \cos\eta, \quad n = \sin\eta \tag{7}$$

Next, the kinetic energy of the composite shaft will be derived. It is assumed here that the size and the shape of the shaft's cross-sections remain unchanged during the motion. For an arbitrarily point P on a typical cross-section of shaft (referring to Fig. 3), its new position (resulting from the axial, bending, transverse shear and torsion deformation, and the spinning of the shaft) can be described by using a set of reference coordinates x'–y'–z' fixed to the cross-section of shaft. According to the above assumption of the cross-sections, the *distance* between point P and the center of the cross-section G will remain the same during the motion. Hence, the displacement vector $\bar{R}_{P/O}$, where point O (it coincides with the centroid G of the cross-section before deformation) is the origin of an inertial Cartesian coordinate system, can be expressed as (Chang and Jan, 1996)

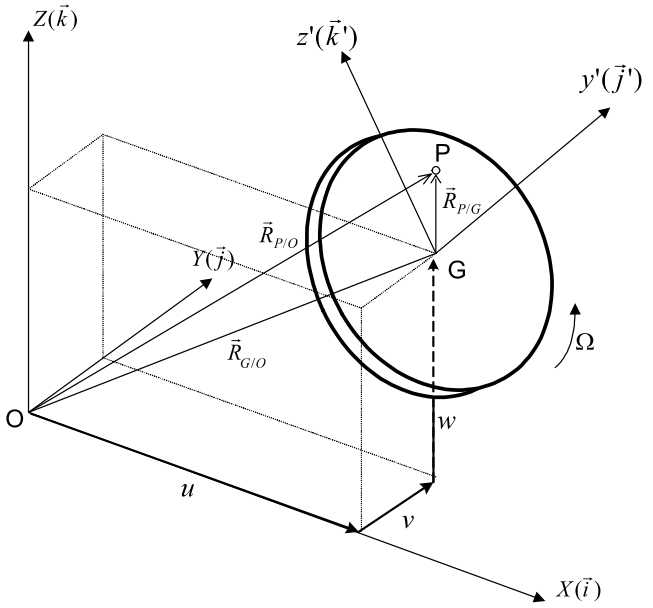

Fig. 3. The displacement of an arbitrary point p on the cross-section of the shaft.

$$\vec{R}_{P/O} = \vec{R}_{G/O} + \vec{R}_{P/G} = \left(u\vec{i} + v\vec{j} + w\vec{k}\right) + \left(y'\vec{j}' + z'\vec{k}'\right) \tag{8}$$

In the above equation $\vec{i}$, $\vec{j}$, $\vec{k}$ are unit vectors of the inertia coordinate system X–Y–Z, and $\vec{i}'$, $\vec{j}'$, $\vec{k}'$ are those of rotating coordinate system x'–y'–z', while u, v, w represent the displacement components of the centroid G of the cross-section of shaft in the X, Y and Z directions due to flexural deformation. By the use of the coordinate transformation, the displacement vector $\vec{R}_{P/O}$ can be expressed in terms of the inertia reference frame X–Y–Z as

$$\begin{aligned}\vec{R}_{P/O} = {} & (u - y'\beta_y\cos\psi + y'\beta_x\sin\psi + z'\beta_y\sin\psi + z'\beta_x\cos\psi)\vec{i} \\ & + (v + y'\cos\psi + y'\beta_x\beta_y\sin\psi - z'\sin\psi + z'\beta_x\beta_y\cos\psi)\vec{j} + (w + y'\sin\psi + z'\cos\psi)\vec{k}\end{aligned} \tag{9}$$

Here β_y, β_x, ψ can be regarded as the 3–2–1 set of Euler's angles and represent the rotation angles of the cross-sections about z, y and x axes respectively (see Fig. 4). The rotation angle ψ can be resolved into two parts as $\psi = \phi + \Omega t$, where ϕ is the angular displacement of the cross-sections due to the torsion deformation of the shaft, and Ω is the spinning speed of shaft, which is assumed constant. On the derivation of Eq. (9), the rotation angles β_x, β_y are assumed small compared with the unity. In the subsequent analysis, the torsion angle ϕ will also be treated as a small quantity compared with the unity (Fig. 4).

In view of Eq. (9), the kinetic energy T_s of the composite shaft can be expressed as

$$\begin{aligned}T_s &= \frac{1}{2}\int_V \rho(\dot{\vec{R}}_{P/O}\cdot\dot{\vec{R}}_{P/O})\mathrm{d}V \\ &= \frac{1}{2}\int_0^L \{I_m(\dot{u}^2 + \dot{v}^2 + \dot{w}^2) + I_d(\dot{\beta}_x^2 + \dot{\beta}_y^2) - 2\Omega I_p\beta_x\dot{\beta}_y + I_p\dot{\phi}^2 + 2\Omega I_p\dot{\phi} + \Omega^2 I_p + \Omega^2 I_d(\beta_x^2 + \beta_y^2)\}\mathrm{d}x\end{aligned} \tag{10}$$

where L is the total length of the shaft, the $2\Omega I_p\beta_x\dot{\beta}_y$ term accounts for the gyroscopic effect, and $I_d(\dot{\beta}_x^2 + \dot{\beta}_y^2)$ represents the rotary inertia effect. The mass quantity I_m denotes the mass per unit length of the shaft, while I_d the diametrical mass of inertia and I_p the polar mass of inertia of the cross-section of the shaft. They are defined as follows:

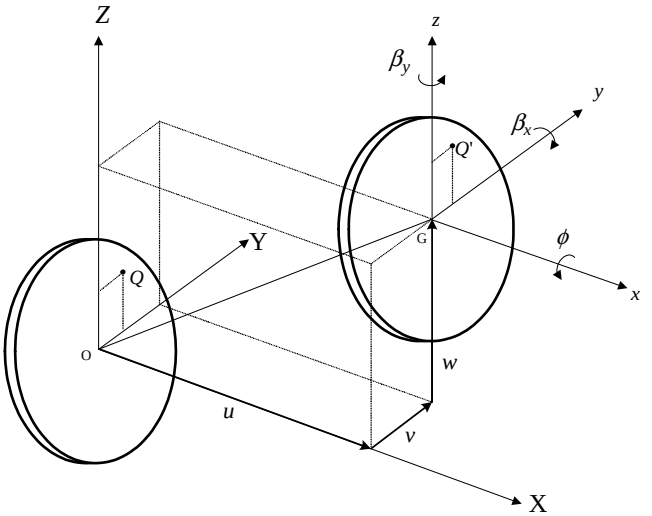

Fig. 4. The elastic displacements of a typical cross-section of the shaft.

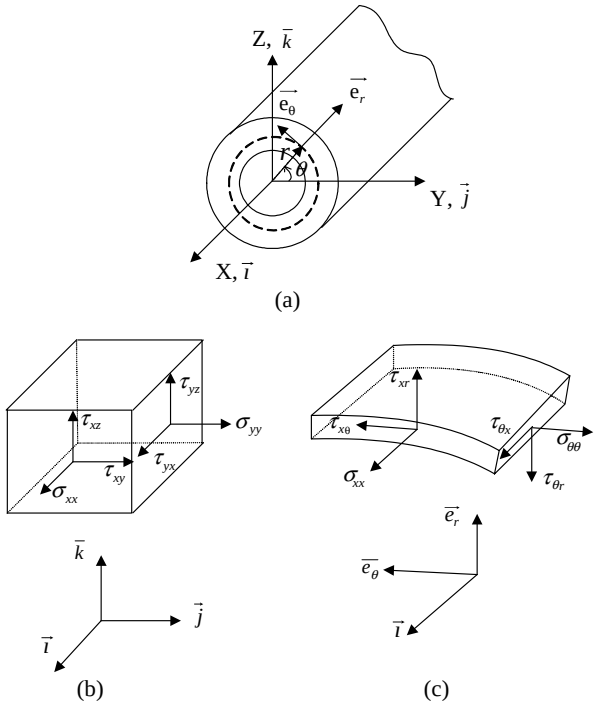

Fig. 5. The employed coordinate systems (a) and the definitions of the stress components (b), (c).

$$
\begin{aligned}
I_{\mathrm{m}} &= \pi \sum_{i=1}^{n} \rho_i (r_{i+1}^2 - r_i^2) \\
I_{\mathrm{d}} &= \frac{\pi}{4} \sum_{i=1}^{n} \rho_i (r_{i+1}^4 - r_i^4) \\
I_{\mathrm{p}} &= \frac{\pi}{2} \sum_{i=1}^{n} \rho_i (r_{i+1}^4 - r_i^4)
\end{aligned}
\tag{11}
$$

Here n is the number of layers in the laminate, and r_i and r_{i+1} are the inner and outer radii of the ith layer. As the $\Omega^2 I_{\mathrm{d}}(\beta_x^2 + \beta_y^2)$ term in Eq. (10) is far smaller than $\Omega^2 I_{\mathrm{p}}$, it will be neglected in the further analysis. By taking the first variation of kinetic energy yields

$$
\begin{aligned}
\delta T_{\mathrm{s}} = \int_0^L \Bigg\{ & I_{\mathrm{m}} \left(\dot{u} \frac{\partial \delta u}{\partial t} + \dot{v} \frac{\partial \delta v}{\partial t} + \dot{w} \frac{\partial \delta w}{\partial t} \right) + I_{\mathrm{d}} \left(\dot{\beta}_x \frac{\partial \delta \beta_x}{\partial t} + \dot{\beta}_y \frac{\partial \delta \beta_y}{\partial t} \right) - I_{\mathrm{p}} \Omega \left(\dot{\beta}_y \delta \beta_x + \beta_x \frac{\partial \delta \beta_y}{\partial t} \right) \\
& + I_{\mathrm{p}} \dot{\phi} \delta \dot{\phi} + I_{\mathrm{p}} \Omega \delta \dot{\phi} \Bigg\} \mathrm{d}x
\end{aligned}
\tag{12}
$$

To derive the strain energy expression of the composite shaft, the following form of the displacement fields of the shaft are assumed.

$$
\begin{aligned}
u_x(x, y, z, t) &= u(x, t) + z\beta_x(x, t) - y\beta_y(x, t) \\
u_y(x, y, z, t) &= v(x, t) - z\phi(x, t) \\
u_z(x, y, z, t) &= w(x, t) + y\phi(x, t)
\end{aligned}
\tag{13}
$$

where u_x, u_y and u_z are the flexural displacements of any point on the cross-section of the shaft in the x, y and z directions. As shown in Fig. 4, the variables u, v and w denote the flexural displacements in the x, y and z directions of the points on the reference axis of the shaft, while ϕ, β_x and β_y are the rotation angles of the cross-section, about the x-, y- and z-axis respectively, due solely to the elastic deformation of the shaft. Here the x–y–z is a coordinate system attached to a translating frame with the origin located at the center of the cross-section such that its axes remain parallel to the inertia reference frame X–Y–Z.

The linear elastic and small deflection theory is adopted in this paper. According to this theory, the linear strain–displacement relations based on the above displacement assumption can be shown to be

$$\begin{aligned}
\varepsilon_{xx} &= \frac{\partial u}{\partial x} + z\frac{\partial \beta_x}{\partial x} - y\frac{\partial \beta_y}{\partial x} \\
\varepsilon_{yy} &= \varepsilon_{zz} = \varepsilon_{yz} = 0 \\
\varepsilon_{xy} &= \frac{1}{2}\left(-\beta_y + \frac{\partial v}{\partial x} - z\frac{\partial \phi}{\partial x}\right) \\
\varepsilon_{xz} &= \frac{1}{2}\left(\beta_x + \frac{\partial w}{\partial x} + y\frac{\partial \phi}{\partial x}\right)
\end{aligned} \tag{14}$$

Since the shapes of the cross-sections of the composite shaft are assumed circular, it is more convenient to express the stress–strain relations of the composite material of the shaft using the cylindrical coordinate system (Fig. 5). The strain components in this coordinate system can be expressed in terms of their counterparts in the Cartesian coordinate system as (see, e.g., a textbook by Fung, 1994)

$$\begin{Bmatrix} \varepsilon_{xx} \\ \varepsilon_{\theta\theta} \\ \varepsilon_{rr} \\ \varepsilon_{x\theta} \\ \varepsilon_{r\theta} \\ \varepsilon_{xr} \end{Bmatrix} = \begin{bmatrix} 1 & 0 & 0 & 0 & 0 & 0 \\ 0 & n^2 & m^2 & 0 & -2mn & 0 \\ 0 & m^2 & n^2 & 0 & 2mn & 0 \\ 0 & 0 & 0 & -n & 0 & m \\ 0 & -mn & mn & 0 & (m^2-n^2) & 0 \\ 0 & 0 & 0 & m & 0 & n \end{bmatrix} \begin{Bmatrix} \varepsilon_{xx} \\ \varepsilon_{yy} \\ \varepsilon_{zz} \\ \varepsilon_{xy} \\ \varepsilon_{yz} \\ \varepsilon_{xz} \end{Bmatrix} \tag{15}$$

Here $m = \cos\theta$ and $n = \sin\theta$. Considering Eqs. (14) and (15) and letting $y = r\cos\theta$, $z = r\sin\theta$, the strain components in the cylindrical coordinate system can be written in terms of the displacement variables defined earlier as

$$\begin{aligned}
\varepsilon_{xx} &= \frac{\partial u}{\partial x} + r\sin\theta\frac{\partial \beta_x}{\partial x} - r\cos\theta\frac{\partial \beta_y}{\partial x} \\
\varepsilon_{x\theta} &= \frac{1}{2}\left(\beta_y\sin\theta + \beta_x\cos\theta - \sin\theta\frac{\partial v}{\partial x} + \cos\theta\frac{\partial w}{\partial x} + r\frac{\partial \phi}{\partial x}\right) \\
\varepsilon_{xr} &= \frac{1}{2}\left(\beta_x\sin\theta - \beta_y\cos\theta + \sin\theta\frac{\partial w}{\partial x} + \cos\theta\frac{\partial v}{\partial x}\right) \varepsilon_{rr} = \varepsilon_{\theta\theta} = \varepsilon_{r\theta} = 0
\end{aligned} \tag{16}$$

The stress–strain relations of the ith layer expressed in the cylindrical coordinate system can be expressed as

$$\begin{aligned}
\sigma_{xx} &= \overline{Q}_{11i}\varepsilon_{xx} + k_s\overline{Q}_{16i}\gamma_{x\theta} \\
\tau_{x\theta} &= k_s\overline{Q}_{16i}\varepsilon_{xx} + k_s\overline{Q}_{66i}\gamma_{x\theta} \\
\tau_{xr} &= k_s\overline{Q}_{55i}\gamma_{xr}
\end{aligned} \tag{17}$$

where k_s is the shear correction factor proposed by Dharmarajan and McCutchen (1973).

The strain energy of the composite shaft U_s can be written as

$$U_s = \frac{1}{2}\int_V [\sigma]^T[\varepsilon]\,dV = \frac{1}{2}\int_V (\sigma_{xx}\varepsilon_{xx} + \sigma_{rr}\varepsilon_{rr} + \sigma_{\theta\theta}\varepsilon_{\theta\theta} + 2\tau_{xr}\varepsilon_{xr} + 2\tau_{x\theta}\varepsilon_{x\theta} + 2\tau_{r\theta}\varepsilon_{r\theta})dV \tag{18}$$

Taking variation of the above strain energy expression and considering Eq. (16), one obtains

$$\begin{aligned}\delta U_s &= \int_V (\sigma_{xx}\delta\varepsilon_{xx} + 2\tau_{xr}\delta\varepsilon_{xr} + 2\tau_{x\theta}\delta\varepsilon_{x\theta})dV \\ &= \int_V \left\{\sigma_{xx}\left(\frac{\partial\delta u}{\partial x} + r\sin\theta\frac{\partial\delta\beta_x}{\partial x} - r\cos\theta\frac{\partial\delta\beta_y}{\partial x}\right) + \tau_{xr}\left(\sin\theta\,\delta\beta_x - \cos\theta\,\delta\beta_y + \cos\theta\frac{\partial\delta v}{\partial x} + \sin\theta\frac{\partial\delta w}{\partial x}\right)\right. \\ &\quad \left. + \tau_{x\theta}\left(\cos\theta\,\delta\beta_x + \sin\theta\,\delta\beta_y - \sin\theta\frac{\partial\delta v}{\partial x} + \cos\theta\frac{\partial\delta w}{\partial x} + r\frac{\partial\delta\phi}{\partial x}\right)\right\}dV\end{aligned} \tag{19}$$

Define the following stress resultants N_x, $Q_{xr}^{(1)}$, $Q_{xr}^{(2)}$, $Q_{x\theta}^{(1)}$, $Q_{x\theta}^{(2)}$ and stress couples M_y, M_z, $M_{x\theta}$ as

$$\begin{aligned}&N_x = \int_A \sigma_{xx}\,dA, \quad M_y = \int_A \sigma_{xx} r\sin\theta\,dA, \\ &M_z = \int_A \sigma_{xx} r\cos\theta\,dA, \quad M_{x\theta} = \int_A \tau_{x\theta} r\,dA, \\ &Q_{xr}^{(1)} = \int_A \tau_{xr}\sin\theta\,dA, \quad Q_{xr}^{(2)} = \int_A \tau_{xr}\cos\theta\,dA, \\ &Q_{x\theta}^{(1)} = \int_A \tau_{x\theta}\sin\theta\,dA, \quad Q_{x\theta}^{(2)} = \int_A \tau_{x\theta}\cos\theta\,dA.\end{aligned} \tag{20}$$

Making use of the variables defined in Eq. (20), Eq. (19) can be written as

$$\begin{aligned}\delta U_s = \int_0^L \left\{N_x\frac{\partial\delta u}{\partial x} + M_y\frac{\partial\delta\beta_x}{\partial x} - M_z\frac{\partial\delta\beta_y}{\partial x} + M_{x\theta}\frac{\partial\delta\phi}{\partial x} + (Q_{xr}^{(1)} + Q_{x\theta}^{(2)})\delta\beta_x - (Q_{xr}^{(2)} - Q_{x\theta}^{(1)})\delta\beta_y\right. \\ \left. + (Q_{xr}^{(2)} - Q_{x\theta}^{(1)})\frac{\partial\delta v}{\partial x} + (Q_{xr}^{(1)} + Q_{x\theta}^{(2)})\frac{\partial\delta w}{\partial x}\right\}dx\end{aligned} \tag{21}$$

Furthermore, by taking into account of Eqs. (16) and (17), the stress resultants and stress couples defined in Eqs. (20) can be expressed in terms of the displacement variables as

$$
\begin{aligned}
N_x &= A_{11}\frac{\partial u}{\partial x} + k_s B_{16}\frac{\partial \phi}{\partial x} \\
M_y &= D_{11}\frac{\partial \beta_x}{\partial x} + \frac{1}{2}k_s B_{16}\left(\beta_y - \frac{\partial v}{\partial x}\right) \\
M_z &= -D_{11}\frac{\partial \beta_y}{\partial x} + \frac{1}{2}k_s B_{16}\left(\beta_x + \frac{\partial w}{\partial x}\right) \\
M_{x\theta} &= k_s B_{16}\frac{\partial u}{\partial x} + k_s D_{66}\frac{\partial \phi}{\partial x} \\
Q_{xr}^{(1)} &= k_s A_{55}\left(\beta_x + \frac{\partial w}{\partial x}\right) \\
Q_{xr}^{(2)} &= k_s A_{55}\left(-\beta_y + \frac{\partial v}{\partial x}\right) \\
Q_{x\theta}^{(1)} &= \frac{1}{2}k_s B_{16}\frac{\partial \beta_x}{\partial x} + k_s A_{66}\left(\beta_y - \frac{\partial v}{\partial x}\right) \\
Q_{x\theta}^{(2)} &= -\frac{1}{2}k_s B_{16}\frac{\partial \beta_y}{\partial x} + k_s A_{66}\left(\beta_x + \frac{\partial w}{\partial x}\right)
\end{aligned}
\tag{22}
$$

in which

$$
\begin{aligned}
A_{11} &= \pi\sum_{i=1}^{n}\overline{Q}_{11i}(r_{i+1}^2 - r_i^2) \\
A_{55} &= \frac{\pi}{2}\sum_{i=1}^{n}\overline{Q}_{55i}(r_{i+1}^2 - r_i^2) \\
A_{66} &= \frac{\pi}{2}\sum_{i=1}^{n}\overline{Q}_{66i}(r_{i+1}^2 - r_i^2) \\
B_{16} &= \frac{2\pi}{3}\sum_{i=1}^{n}\overline{Q}_{16i}(r_{i+1}^3 - r_i^3) \\
D_{11} &= \frac{\pi}{4}\sum_{i=1}^{n}\overline{Q}_{11i}(r_{i+1}^4 - r_i^4) \\
D_{66} &= \frac{\pi}{2}\sum_{i=1}^{n}\overline{Q}_{66i}(r_{i+1}^4 - r_i^4)
\end{aligned}
\tag{23}
$$

2.2. Kinetic energy of disks

The disks fixed to the shaft are assumed rigid and made of isotropic materials. According to Eq. (10) the kinetic energy of the disks can be expressed as

$$
T_D = \frac{1}{2}\int_0^L \sum_{j=1}^{n_D}\left\{I_{mj}^D(\dot{u}^2 + \dot{v}^2 + \dot{w}^2) + I_{dj}^D(\dot{\beta}_x^2 + \dot{\beta}_y^2) - 2\Omega I_{dj}^D\beta_x\dot{\beta}_y + I_{pj}^D\dot{\phi}^2 + 2\Omega I_{pj}^D\dot{\phi} + \Omega^2 I_{pj}^D\right\}\Delta(x - x_{Dj})\mathrm{d}x
\tag{24}
$$

where I_{mj}^D, I_{dj}^D and I_{pj}^D are the mass, the diametrical mass moment of inertia and the polar mass moment of inertia of the disk j. The symbol $\Delta(x - x_{Dj})$ denotes the one-dimensional spatial Dirac delta function, n_D the number of the discrete disks attached to the shaft and x_{Dj} the location of the jth disk. Taking variation of T_D yields

$$\delta T_{\mathrm{D}} = \int_0^L \sum_{j=1}^{n_{\mathrm{D}}} \left\{ I_{\mathrm{m}j}^{\mathrm{D}} \left(\dot{u} \frac{\partial \delta u}{\partial t} + \dot{v} \frac{\partial \delta v}{\partial t} + \dot{w} \frac{\partial \delta w}{\partial t} \right) + I_{\mathrm{d}j}^{\mathrm{D}} \left(\dot{\beta}_x \frac{\partial \delta \beta_x}{\partial t} + \dot{\beta}_y \frac{\partial \delta \beta_y}{\partial t} \right) - I_{\mathrm{p}j}^{\mathrm{D}} \Omega \left(\dot{\beta}_y \delta \beta_x + \beta_x \frac{\partial \delta \beta_y}{\partial t} \right) + I_{\mathrm{p}j}^{\mathrm{D}} \dot{\phi} \delta \dot{\phi} + I_{\mathrm{p}j}^{\mathrm{D}} \Omega \delta \dot{\phi} \right\} \Delta(x - x_{\mathrm{D}j}) \mathrm{d}x \tag{25}$$

2.3. Work of external loads and bearings

Supposed that the shaft is subjected to external force intensities (force per unit length) p_x, p_y and p_z, and external torque intensities (moment per unit length) Γ_x, Γ_y and $\Gamma_{x\theta}$ distributed along the shaft. All external loads are assumed to be functions of x and t. Then the virtual work done by these external loads can be written as

$$\delta W_{\mathrm{e}} = \int_0^L (p_x \delta u + p_y \delta v + p_z \delta w + \Gamma_x \delta \beta_x + \Gamma_y \delta \beta_y + \Gamma_{x\theta} \delta \phi) \mathrm{d}x \tag{26a}$$

The stiffness and damping effects of the bearings are modeled using springs and viscous dampers. The virtual work done by these elements can be expressed as (Lalanne and Ferraris, 1990)

$$\delta W_{\mathrm{b}} = \int_0^L \sum_{j=1}^{n_{\mathrm{b}}} (-K_{YY}^{\mathrm{b}j} v \delta v - K_{ZY}^{\mathrm{b}j} v \delta w - K_{YZ}^{\mathrm{b}j} w \delta v - K_{ZZ}^{\mathrm{b}j} w \delta w - C_{YY}^{\mathrm{b}j} \dot{v} \delta \dot{v} - C_{ZY}^{\mathrm{b}j} \dot{v} \delta \dot{w} - C_{YZ}^{\mathrm{b}j} \dot{w} \delta \dot{v} - C_{ZZ}^{\mathrm{b}j} \dot{w} \delta \dot{w}) \times \Delta(x - x_{\mathrm{b}j}) \mathrm{d}x \tag{26b}$$

Here n_{b} denotes the number of the bearings, $x_{\mathrm{b}j}$ the location, and $K^{\mathrm{b}j}$ and $C^{\mathrm{b}j}$ the equivalent stiffness and damping coefficients of the jth bearings.

2.4. Governing equations of system

By taking into account of the energy expressions derived above and invoking the extended Hamilton's principle (see, e.g., Meirovitch, 1990), which is

$$\int_{t_1}^{t_2} [\delta(T_{\mathrm{s}} + T_{\mathrm{D}}) - \delta U_{\mathrm{s}} + \delta W_{\mathrm{b}} + \delta W_{\mathrm{e}}] \mathrm{d}t = 0 \tag{27}$$

The equations of the motion can be shown to be the following:

$$\begin{aligned}
&\delta u: \ I_{\mathrm{m}} \frac{\partial^2 u}{\partial t^2} - \frac{\partial N_x}{\partial x} + \sum_{j=1}^{n_{\mathrm{D}}} I_{\mathrm{m}j}^{\mathrm{D}} \frac{\partial^2 u}{\partial t^2} \Delta(x - x_{\mathrm{D}j}) = p_x \\
&\delta v: \ I_{\mathrm{m}} \frac{\partial^2 v}{\partial t^2} + \frac{\partial Q_{x\theta}^{(1)}}{\partial x} - \frac{\partial Q_{xr}^{(2)}}{\partial x} + \sum_{j=1}^{n_{\mathrm{D}}} I_{\mathrm{m}j}^{\mathrm{D}} \frac{\partial^2 v}{\partial t^2} \Delta(x - x_{\mathrm{D}j}) + F_V^{\mathrm{b}} = p_y \\
&\delta w: \ I_{\mathrm{m}} \frac{\partial^2 w}{\partial t^2} - \frac{\partial Q_{x\theta}^{(2)}}{\partial x} - \frac{\partial Q_{xr}^{(1)}}{\partial x} + \sum_{j=1}^{n_{\mathrm{D}}} I_{\mathrm{m}j}^{\mathrm{D}} \frac{\partial^2 w}{\partial t^2} \Delta(x - x_{\mathrm{D}j}) + F_W^{\mathrm{b}} = P_z \\
&\delta \beta_x: \ I_{\mathrm{d}} \frac{\partial^2 \beta_x}{\partial t^2} + I_{\mathrm{p}} \Omega \frac{\partial \beta_y}{\partial t} - \frac{\partial M_y}{\partial x} + Q_{x\theta}^{(2)} + Q_{xr}^{(1)} + \sum_{j=1}^{n_{\mathrm{D}}} I_{\mathrm{d}j}^{\mathrm{D}} \frac{\partial^2 \beta_x}{\partial t^2} \Delta(x - x_{\mathrm{D}j}) = \Gamma_x \\
&\delta \beta_y: \ I_{\mathrm{d}} \frac{\partial^2 \beta_y}{\partial t^2} - I_{\mathrm{p}} \Omega \frac{\partial \beta_x}{\partial t} + \frac{\partial M_z}{\partial x} + Q_{x\theta}^{(1)} - Q_{xr}^{(2)} + \sum_{j=1}^{n_{\mathrm{D}}} I_{\mathrm{d}j}^{\mathrm{D}} \frac{\partial^2 \beta_y}{\partial t^2} \Delta(x - x_{\mathrm{D}j}) = \Gamma_y \\
&\delta \phi: \ I_{\mathrm{p}} \frac{\partial^2 \phi}{\partial t^2} - \frac{\partial M_{x\theta}}{\partial x} + \sum_{j=1}^{n_{\mathrm{D}}} I_{\mathrm{p}j}^{\mathrm{D}} \frac{\partial^2 \phi}{\partial t^2} \Delta(x - x_{\mathrm{D}j}) = \Gamma_{x\theta}
\end{aligned} \tag{28a}$$

where

$$F_V^{\mathrm{b}} = \sum_{j=1}^{n_{\mathrm{b}}} \left(K_{YY}^{\mathrm{b}j} v + K_{YZ}^{\mathrm{b}j} w + C_{YY}^{\mathrm{b}j} \dot{v} + C_{YZ}^{\mathrm{b}j} \dot{w} \right) \Delta(x - x_{\mathrm{b}j})$$
$$F_W^{\mathrm{b}} = \sum_{j=1}^{n_{\mathrm{b}}} \left(K_{ZZ}^{\mathrm{b}j} w + K_{ZY}^{\mathrm{b}j} v + C_{ZZ}^{\mathrm{b}j} \dot{w} + C_{ZY}^{\mathrm{b}j} \dot{v} \right) \Delta(x - x_{\mathrm{b}j}) \tag{28b}$$

In view of Eq. (28a) and the stress resultant–displacement and stress couple–displacement relations, Eq. (22), the governing equations of the composite shaft systems can be shown to be the following:

$$\delta u: \; I_{\mathrm{m}} \frac{\partial^2 u}{\partial t^2} - A_{11} \frac{\partial^2 u}{\partial x^2} - k_{\mathrm{s}} B_{16} \frac{\partial^2 \phi}{\partial x^2} + \sum_{j=1}^{n_{\mathrm{D}}} I_{\mathrm{m}j}^{\mathrm{D}} \frac{\partial^2 u}{\partial t^2} \Delta(x - x_{\mathrm{D}j}) = p_x$$

$$\delta v: \; I_{\mathrm{m}} \frac{\partial^2 v}{\partial t^2} + k_{\mathrm{s}}(A_{55} + A_{66}) \left(\frac{\partial \beta_y}{\partial x} - \frac{\partial^2 v}{\partial x^2} \right) + \frac{1}{2} k_{\mathrm{s}} B_{16}^2 \frac{\partial^2 \beta_x}{\partial x^2} + \sum_{j=1}^{n_{\mathrm{D}}} I_{\mathrm{m}j}^{\mathrm{D}} \frac{\partial^2 v}{\partial t^2} \Delta(x - x_{\mathrm{D}j}) + F_V^{\mathrm{b}} = p_y$$

$$\delta w: \; I_{\mathrm{m}} \frac{\partial^2 w}{\partial t^2} - k_{\mathrm{s}}(A_{55} + A_{66}) \left(\frac{\partial^2 w}{\partial x^2} + \frac{\partial \beta_x}{\partial x} \right) - \frac{1}{2} k_{\mathrm{s}} B_{16} \frac{\partial^2 \beta_y}{\partial x^2} + \sum_{j=1}^{n_{\mathrm{D}}} I_{\mathrm{m}j}^{\mathrm{D}} \frac{\partial^2 w}{\partial t^2} \Delta(x - x_{\mathrm{D}j}) + F_W^{\mathrm{b}} = P_z$$

$$\delta \beta_x: \; I_{\mathrm{d}} \frac{\partial^2 \beta_x}{\partial t^2} + I_{\mathrm{p}} \Omega \frac{\partial \beta_y}{\partial t} + \frac{1}{2} k_{\mathrm{s}} B_{16} \frac{\partial^2 v}{\partial x^2} - D_{11} \frac{\partial^2 \beta_x}{\partial x^2} + k_{\mathrm{s}}(A_{55} + A_{66}) \left(\frac{\partial w}{\partial x} + \beta_x \right)$$
$$- k_{\mathrm{s}} B_{16} \frac{\partial \beta_y}{\partial x} + \sum_{j=1}^{n_{\mathrm{D}}} I_{\mathrm{d}j}^{\mathrm{D}} \frac{\partial^2 \beta_x}{\partial t^2} \Delta(x - x_{\mathrm{D}j}) = \Gamma_x \tag{29}$$

$$\delta \beta_y: \; I_{\mathrm{d}} \frac{\partial^2 \beta_y}{\partial t^2} + I_{\mathrm{p}} \Omega \frac{\partial \beta_x}{\partial t} + \frac{1}{2} k_{\mathrm{s}} B_{16}^2 \frac{\partial w}{\partial x^2} - D_{11} \frac{\partial^2 \beta_y}{\partial x^2} - k_{\mathrm{s}}(A_{55} + A_{66}) \left(\frac{\partial v}{\partial x} - \beta_y \right) + k_{\mathrm{s}} B_{16} \frac{\partial \beta_x}{\partial x}$$
$$+ \sum_{j=1}^{n_{\mathrm{D}}} I_{\mathrm{d}j}^{\mathrm{D}} \frac{\partial^2 \beta_y}{\partial t^2} \Delta(x - x_{\mathrm{D}j}) = \Gamma_y$$

$$\delta \phi: \; I_{\mathrm{p}} \frac{\partial^2 \phi}{\partial t^2} - k_{\mathrm{s}} B_{16} \frac{\partial^2 u}{\partial x^2} - k_{\mathrm{s}} D_{66} \frac{\partial^2 \phi}{\partial x^2} + \sum_{j=1}^{n_{\mathrm{D}}} I_{\mathrm{p}j}^{\mathrm{D}} \frac{\partial^2 \phi}{\partial t^2} \Delta(x - x_{\mathrm{D}j}) = \Gamma_{x\theta}$$

The boundary conditions of the system are defined by specifying at both ends of the shaft the value of only one variable from each pair of the following six pairs of variables: (N_x, u), (Q_y, v), (Q_z, w), (M_y, β_x), (M_z, β_y), and $(M_{x\theta}, \phi)$. Here $Q_y = Q_{xr}^{(2)} - Q_{x\theta}^{(1)}$ and $Q_z = Q_{xr}^{(1)} + Q_{x\theta}^{(2)}$.

Next, the analysis of responses of the spinning shaft's systems based on the above shaft model will be discussed.

2.5. Approximate solution method

The finite element method is used here to find the approximate solution of the system. By employing this method, the governing equations are approximated by a system of ordinary differential equations. In the present finite element model, the three-node one-dimensional line elements, each node having 6 degrees of freedom, interpolated using Lagrangian interpolation functions are used to approximate the displacement fields of shaft. The displacement field variables can then be expressed as

$$
\begin{aligned}
u &= \sum_{i=1}^{3} u^i(t)\varphi_i(x), \quad \beta_x = \sum_{i=1}^{3} \beta_x^i(t)\varphi_i(x) \\
v &= \sum_{i=1}^{3} v^i(t)\varphi_i(x), \quad \beta_y = \sum_{i=1}^{3} \beta_y^i(t)\varphi_i(x) \\
w &= \sum_{i=1}^{3} w^i(t)\varphi_i(x), \quad \phi = \sum_{i=1}^{3} \phi^i(t)\varphi_i(x)
\end{aligned} \tag{30}
$$

in which

$$
\varphi_1 = \frac{-\xi(1-\xi)}{2}, \quad \varphi_2 = 1-\xi^2, \quad \varphi_3 = \frac{\xi(1+\xi)}{2}.
$$

The φ_i, $i = 1, 2, 3$, are the interpolation functions and ξ is the natural coordinate whose values varies between -1 and 1. Substituting the above expressions of displacement variables into the governing equations and applying the Galerkin procedure, the following matrix equations of motion of the spinning shaft system can be found.

$$
[M]\{\ddot{q}\} + (\Omega[G] + [C])\{\dot{q}\} + [K]\{q\} = \{F\} \tag{31}
$$

where $[M]$ represents the mass matrix, $[G]$ the gyroscopic matrix, $[C]$ the damping matrix, $[K]$ the stiffness matrix, $\{F\}$ the external force vector and $\{q\}$ the displacement vector. The detailed expressions of these matrices can be found in Appendix A.

The damping matrix $[C]$ has included in addition to the viscous damping of the bearings the proportional viscous damping of the shaft. It can be expressed as

$$
[C] = [C_{\mathrm{b}}] + [C_{\mathrm{p}}] \tag{32a}
$$

where

$$
[C_{\mathrm{p}}] = [M][\Phi][\widetilde{C}][\Phi]^{\mathrm{T}}[M] \tag{32b}
$$

and denotes the proportional viscous damping matrix. The matrix $[\Phi]$ is the modal matrix such that

$$
[\Phi]^{\mathrm{T}}[M][\Phi] = [I], \quad [\Phi]^{\mathrm{T}}[K][\Phi] = [\Lambda] \tag{33a,b}
$$

and

$$
[\widetilde{C}] = \begin{bmatrix}
2\zeta_1\omega_1 & & & & \\
& 2\zeta_2\omega_2 & & 0 & \\
& & 2\zeta_3\omega_3 & & \\
& 0 & & \ddots & \\
& & & & 2\zeta_N\omega_N
\end{bmatrix} \tag{33c}
$$

in which ω_i and ς_i are the natural frequencies of the undamped non-rotating shaft system and the modal damping ratios respectively.

In the following section the responses of the spinning composite shaft system are studied based on the approximate equations of motion, Eq. (31).

3. Numerical examples

In the following examples, first, the lowest critical speeds of composite shafts are analyzed and compared with those available in the literature to verify the present model. Several methods can be used to determine the critical speeds of a rotating shaft. They include the commonly known Campbell diagram method (see e.g., Lalanne and Ferraris, 1990), as well as the whirling frame method (only suitable for the undamped systems) and the sensitivity method. The latter two methods were developed by Nelson and Mcvaugh (1976) and Nelson et al. (1986), and are adopted in this paper.

In the first example, the composite hollow shafts made of boron/epoxy laminae, which are considered by Bert and Kim (1995), are investigated. The properties of the material are listed in Table 1. The shaft has a total length of 2.47 m. The mean diameter D and the wall thickness of the shaft are 12.69 cm and 1.321 mm respectively. The lay-up is $[90°/45°/-45°/0°_6/90°]$ starting from the inside surface of the hollow shaft. A shear correction factor of 0.503 is also used. The shaft is modeled by 20 finite elements of equal length. The supporting bearings are modeled as springs whose stiffness are $K_{yy} = K_{zz} = 1740$ GN/m and $K_{yz} = K_{zy} = 0$. The result obtained using the present model is shown in Table 2 together with those of referenced papers. As can be seen from the table our results are close to those predicted by other beam theories. Since in the studied example the wall of the shaft is relatively thin, models based on shell theories (Kim and Bert, 1993) are expected to yield more accurate results. In the present example, the critical speed measured from the experiment however is still underestimated by using the Sander shell theory while overestimated by the

Table 1
Properties of composite materials (Bert and Kim, 1995)

	Boron–epoxy	Graphite–epoxy
E_{11} (GPa)	211.0	139.0
E_{22} (GPa)	24.1	11.0
$G_{12} = G_{13}$ (GPa)	6.9	6.05
G_{23} (GPa)	6.9	3.78
ν_{12}	0.36	0.313
Density (kg/m^3)	1967.0	1578.0

Table 2
The critical speed of the boron–epoxy composite shaft

	Theory or method	First critical speed (rpm)
Zinberg and Symonds (1970)	Measured experimentally	6000
	EMBT	5780
dos Reis et al. (1987)	Bernoulli–Euler beam theory with stiffness determined by shell finite elements	4942
Kim and Bert (1993)	Sanders shell theory	5872
	Donnell shallow shell theory	6399
Bert (1992)	Bernoulli–Euler beam theory	5919
Bert and Kim (1995)	Bresse–Timoshenko beam theory	5788
Singh and Gupta (1996)	EMBT	5747
	LBT	5620
Present	Continuum based Timoshenko beam theory	5762

Donnell shallow shell theory. When the material of the shaft is changed to the graphite–epoxy given in Table 1 with other conditions left unchanged, the critical speed obtained from the present model is shown in Table 3. In this case, the result from the present model is compatible to that of the Bresse–Timoshenko beam theory of Bert and Kim (1995).

Next, comparisons are made with those of Bert and Kim (1995) for different length to mean diameter ratios, L/D. The shafts being analyzed are made of the graphite–epoxy material given in Table 1 and all have the same lamination [90°/45°/−45°/0°$_6$/90°]. The mean diameter and the wall thickness of the shaft remain the same as the previous examples. The shear correction factor being used is again 0.503. The results are listed in Table 4. Further results being compared are for generalized orthotropic composite tube of different lamination angles η. The results are shown in Table 5.

From the thin-walled shaft systems studied above, the present shaft model yields results in all cases close to those of the model of Bert and Kim (1995) based on the Bresse–Timoshenko theory. One should stress here that the present model is not only applicable to the thin-walled composite shafts as studied above, but also to the thick-walled shafts as well as to the solid ones.

Table 3
The critical speed of the graphite–epoxy composite shaft

	Theory	First critical speed (rpm)
Bert and Kim (1995)	Sanders shell theory	5349
	Donnell shallow shell theory	5805
	Bernoulli–Euler beam theory	5302
	Bresse–Timoshenko beam theory	5113
Present	Continuum-based Timoshenko beam theory	5197

Table 4
The critical speed (rpm) of graphite–epoxy composite shaft for various length to mean diameter ratios

Theory		L/D							
		2	5	10	15	20	25	30	35
Bert and Kim (1995)	Sanders shell	112,400	41,680	16,450	8585	5183	3441	2440	1816
	Bernoulli–Euler	329,600	76,820	20210	9072	5121	3283	2282	1677
	Bresse–Timoshenko	176,300	54,830	17,880	8543	4945	3209	2246	1658
Present		181,996	55,706	17,929	8527	4925	3192	2233	1648

Table 5
The critical speeds (rpm) of the generally orthotropic of graphite–epoxy composite shaft for various lamination angles

Theory		Lamination angle η (°)						
		0	15	30	45	60	75	90
Bert and Kim (1995)	Sanders shell	5527	4365	3308	2386	2120	2020	1997
	Bermoulli–Euler	6425	5393	4269	3171	2292	1885	1813
	Bresse–Timoshenko	6072	5209	4197	3143	2278	1874	1803
Present		6072	5331	4206	3124	2284	1890	1816

In the following example, the frequencies, mode shapes, as well as the transient response, of a graphite–epoxy composite shaft system are analyzed. The material properties are those listed in Table 1. The lamination scheme of the shaft remains the same as previous examples, while its geometric properties, the properties of a uniform rigid disk, and the properties of the springs and viscous dampers modeling the support conditions are listed in Table 6. The disk is placed at the mid-span of the shaft and assumed its center of mass have a small distance of eccentricity e away its geometric center. The shaft system is shown in Fig. 6. For the finite element analysis, the shaft is divided into 6 elements of equal length.

First, the Campbell diagram containing the frequencies of the first five pairs of bending whirling modes of the above composite system is shown in Fig. 7. Denote the ratio of the whirling bending frequency and the rotation speed of shaft as γ. The intersection point of the line $\gamma = 1$ with the whirling frequency curves indicate the speed at which the shaft will vibrate violently (i.e., the critical speed). In Fig. 7 the second pair of the forward and backward whirling frequencies falls more wide apart in contrast to other pairs of whirling modes. This might be due to the coupling of the pitching motion of the disk with the transverse vibration of shaft. Note that the disk is located at the mid-span of the shaft, while the second whirling forward and backward bending modes are skew-symmetric with respect to the mid-span of the shaft as shown Fig. 9. Next, consider the case that the shaft starts from rest and assume it instantly arrives at the speed of 6000 rpm. The first 10 eigenvalues that correspond to 5 forward (F) and 5 backward (B) whirling bending modes of the shaft running at 6000 rpm are listed in Table 7. The mode shapes corresponding to these eigenvalues modes are illustrated in Figs. 8–12. In these figures, the modes are shown in the

Table 6
The dimensions and properties of the composite shaft system

	Shaft	Disk	Bearings
Total length (m)	0.72		
Modal damping ratios	0.01		
Inner diameter (m)	0.028		
Outer diameter (m)	0.048		
Shear correction factor	0.56		
I_m^D (kg)		2.4364	
e (10^{-5} m)		5.0	
I_p^D (kg m^2)		0.3778	
I_d^D (kg m^2)		0.1901	
$K_{yy} = K_{zz}$ (10^7 N/m)			1.75
$C_{yy} = C_{zz}$ (10^2 N s/m)			5.0

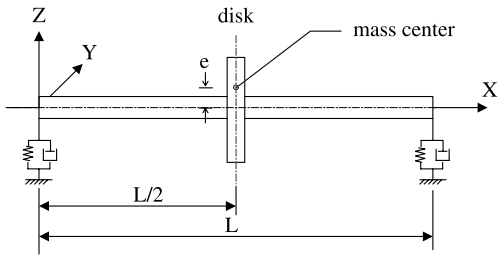

Fig. 6. A bearings-supported flexible shaft containing a rigid disk.

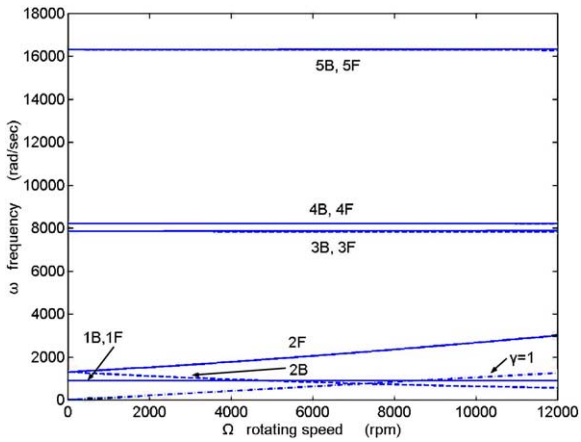

Fig. 7. The Campbell diagram of a composite shaft system ((—) forward modes, (- - -) backward modes).

Table 7
The eigenvalues corresponding to the lowest five forward and backward whirling bending modes of the composite shaft running at 6000 rpm

Mode	Real part	Imaginary part
1B	−9.985	902.867
1F	−9.996	903.566
2B	−8.530	826.702
2F	−21.681	2048.076
3B	−423.449	7841.506
3F	−423.385	7868.068
4B	−484.578	8215.352
4F	−484.748	8218.171
5B	−1513.563	16305.428
5F	−1511.597	16332.143

three-dimensional reference frame as well as in two-dimensional projected views. It can be seen that the first and fourth modes are symmetric while others are the anti-symmetric bending modes.

Lastly, the transient response of the above composite shaft system is illustrated. The vibration of the shaft is caused by the centrifugal force resulting from the unbalanced rigid disk. For the purpose of the verification of the numerical results, the transient response of the composite shaft is obtained by using two different approaches. In the first method, the transient response is obtained by integrating directly the finite element equation, Eq. (31), using the Newmark-β algorithm, while in the second approach, Eq. (31) is solved using the modal analysis method as was done in Chang and Jan (1996). The steady state response of the shaft determined by the method proposed by Nelson and Mcvaugh (1976) is also shown in the figures for comparison. In the simulation, the time step of 0.0002 s is adopted in both Newmark-β and the modal analysis methods. The first four pairs of forward and bending whirling modes in Table 7 are considered in the modal analysis method. The total time-interval of simulation is 0.24 s. The transverse displacements of the geometric center of the disk in the directions of the inertia coordinate Y and Z obtained respectively using the above two methods are plotted in Figs. 13 and 14. The two figures look very similar. It can be seen

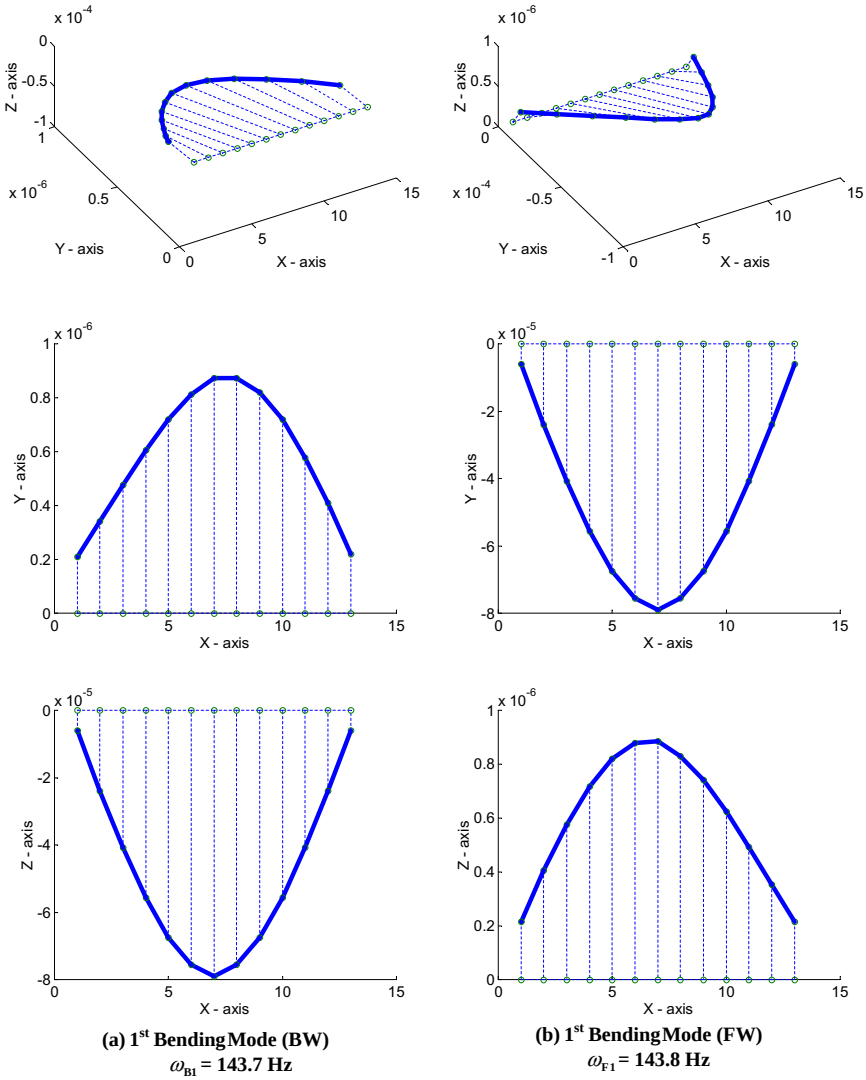

(a) 1st Bending Mode (BW)
ω_{B1} = 143.7 Hz

(b) 1st Bending Mode (FW)
ω_{F1} = 143.8 Hz

Fig. 8. The first backward (a) and forward (b) whirling bending mode shapes of a composite shaft system running at 6000 rpm.

from the figures that though the transient response starts with a fluctuation of displacement, it converges quite rapidly to the steady response as a result of the damping action.

4. Concluding remarks

A simple composite spinning shaft model is presented in this paper. By employing multiple transformations of coordinate systems, a spinning isotropic shaft model considered previously by Chang and Jan (1996) is extended here to the case of laminated composite shafts. It has been demonstrated that our continuum-based beam model is compatible to some beam theories available in the literatures. The present model can be served as a viable alternative for the vibration analysis of the spinning laminated composite shafts.

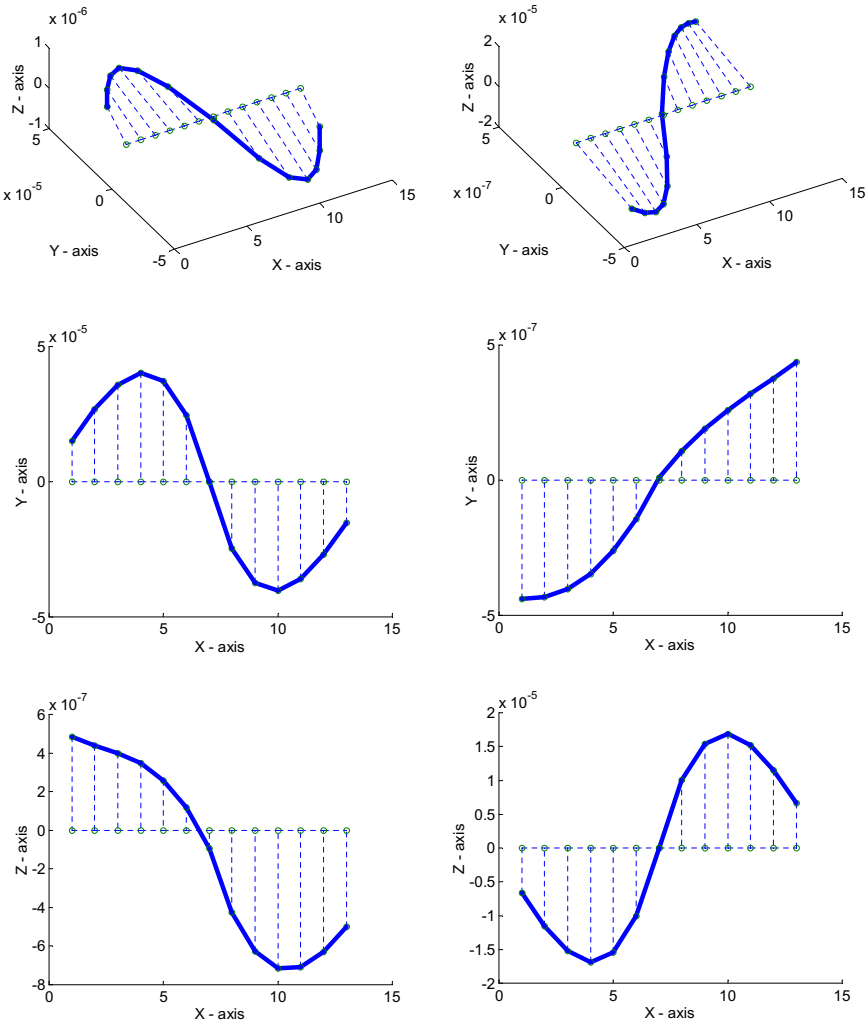

(c) 2nd Bending Mode (BW)
ω_{B2} **= 131.6 Hz**

(d) 2nd Bending Mode (FW)
ω_{F2} **= 325.9 Hz**

Fig. 9. The second backward (c) and forward (d) whirling bending mode shapes of a composite shaft system running at 6000 rpm.

Acknowledgements

The financial support of the research by National Science Council of ROC through projects NSC86-2212-E-005-005 and NSC89-2212-E-005-028 is gratefully acknowledged.

Appendix A. Mass, gyroscopic and stiffness matrices of the laminated composite shaft elements

The nodal generalized displacements $\{q^e\}$ is a column matrix whose transpose is defined as

$$\{q^e\}^T = \left\{ \{U^e\}^T \{V^e\}^T \{W^e\} \{\beta_x^e\}^T \{\beta_y^e\}^T \{\phi^e\}^T \right\}_{1\times 18}$$

The corresponding element matrices are as follows:

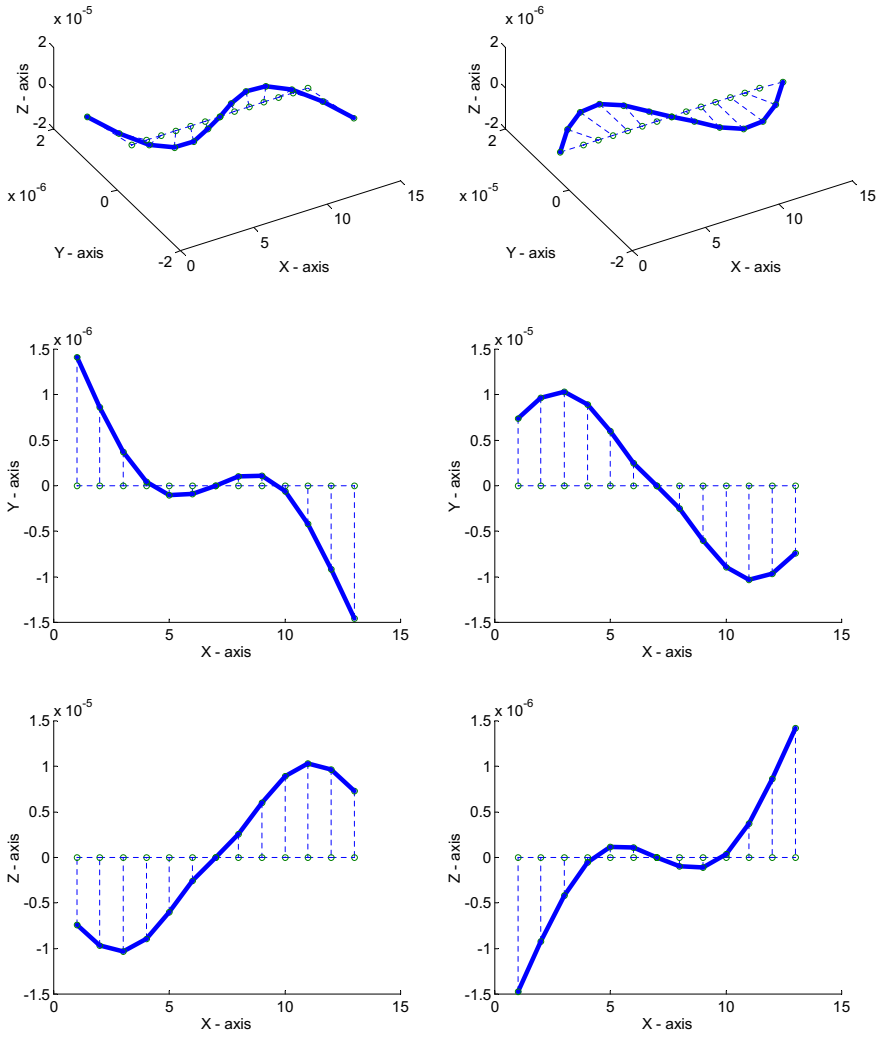

(e) 3rd Bending Mode (BW)
ω_{B3} = 1249.8 Hz

(f) 3rd Bending Mode (FW)
ω_{F3} = 1254.1 Hz

Fig. 10. The third backward (e) and forward (f) whirling bending mode shapes of a composite shaft system running at 6000 rpm.

A.1. Mass matrix

$$[M^e] = \begin{bmatrix} [M^{11}]_{3\times3} & [0]_{3\times3} & [0]_{3\times3} & [0]_{3\times3} & [0]_{3\times3} & [0]_{3\times3} \\ [0]_{3\times3} & [M^{22}]_{3\times3} & [0]_{3\times3} & [0]_{3\times3} & [0]_{3\times3} & [0]_{3\times3} \\ [0]_{3\times3} & [0]_{3\times3} & [M^{33}]_{3\times3} & [0]_{3\times3} & [0]_{3\times3} & [0]_{3\times3} \\ [0]_{3\times3} & [0]_{3\times3} & [0]_{3\times3} & [M^{44}]_{3\times3} & [0]_{3\times3} & [0]_{3\times3} \\ [0]_{3\times3} & [0]_{3\times3} & [0]_{3\times3} & [0]_{3\times3} & [M^{55}]_{3\times3} & [0]_{3\times3} \\ [0]_{3\times3} & [0]_{3\times3} & [0]_{3\times3} & [0]_{3\times3} & [0]_{3\times3} & [M^{66}]_{3\times3} \end{bmatrix}_{18\times18}$$

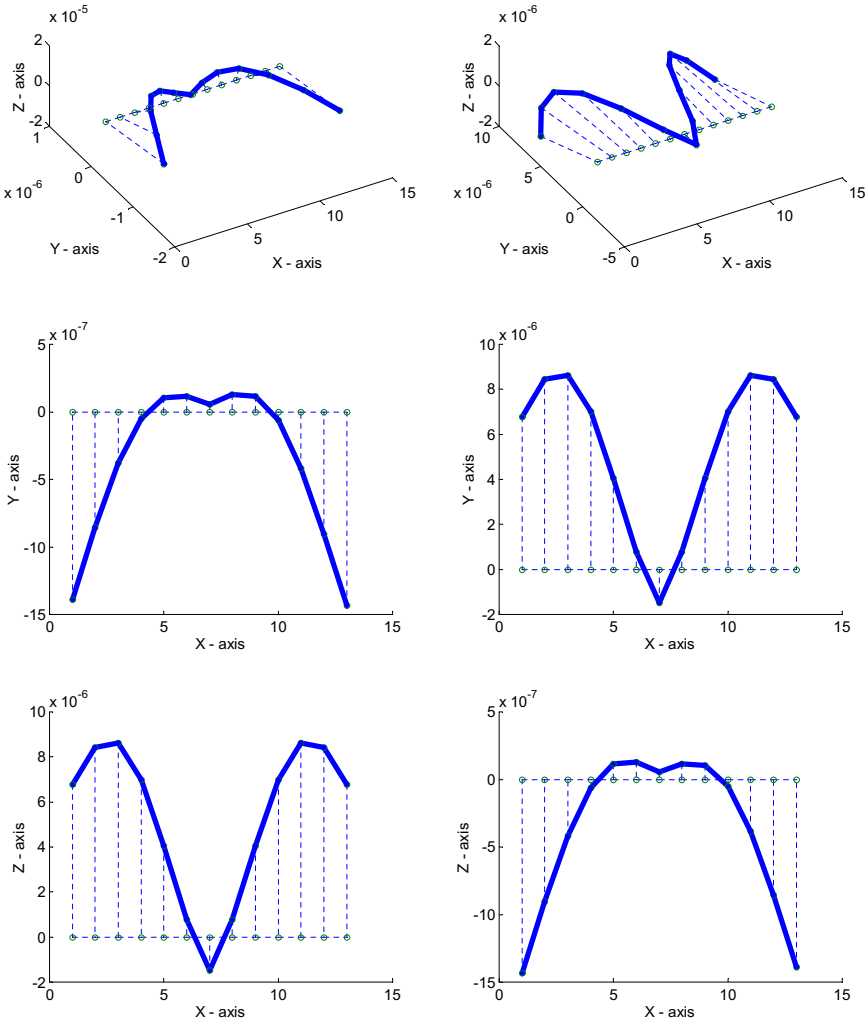

(g) 4th Bending Mode (BW)
ω_{B4} = 1309.8 Hz

(h) 4th Bending Mode (FW)
ω_{F4} = 1310.2 Hz

Fig. 11. The fourth backward (g) and forward (h) whirling bending mode shapes of a composite shaft system running at 6000 rpm.

in which

$$M_{ij}^{11} = \int_{x_a}^{x_b} I_{\mathrm{m}} \varphi_i \varphi_j \,\mathrm{d}x + \int_{x_a}^{x_b} \sum_{k=1}^{n_{\mathrm{D}}} I_{\mathrm{m}}^{\mathrm{D}} \varphi_i \varphi_j \Delta(x - x_{\mathrm{D}k}) \mathrm{d}x$$

$$M_{ij}^{22} = \int_{x_a}^{x_b} I_{\mathrm{m}} \varphi_i \varphi_j \,\mathrm{d}x + \int_{x_a}^{x_b} \sum_{k=1}^{n_{\mathrm{D}}} I_{\mathrm{m}}^{\mathrm{D}} \varphi_i \varphi_j \Delta(x - x_{\mathrm{D}k}) \mathrm{d}x$$

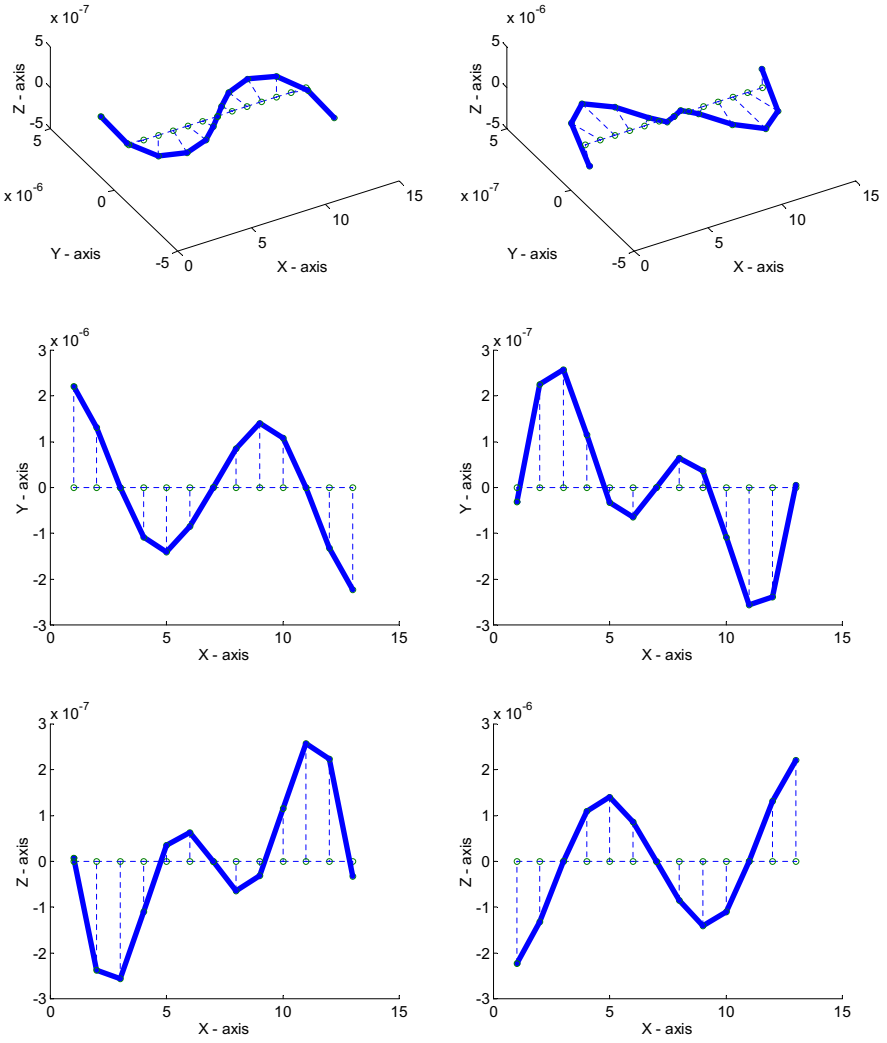

(i) **5th Bending Mode (BW)** ω_{B5} **= 2606.3 Hz**

(j) **5th Bending Mode (FW)** ω_{F5} **= 2610.5 Hz**

Fig. 12. The fifth backward (i) and forward (j) whirling bending mode shapes of a composite shaft system running at 6000 rpm.

$$M_{ij}^{33} = \int_{x_a}^{x_b} I_{\mathrm{m}} \varphi_i \varphi_j \,\mathrm{d}x + \int_{x_a}^{x_b} \sum_{k=1}^{n_{\mathrm{D}}} I_{\mathrm{m}}^{\mathrm{D}} \varphi_i \varphi_j \Delta(x - x_{\mathrm{D}k}) \mathrm{d}x$$

$$M_{ij}^{44} = \int_{x_a}^{x_b} I_{\mathrm{d}} \varphi_i \varphi_j \,\mathrm{d}x + \int_{x_a}^{x_b} \sum_{k=1}^{n_{\mathrm{D}}} I_{\mathrm{d}}^{\mathrm{D}} \varphi_i \varphi_j \Delta(x - x_{\mathrm{D}k}) \mathrm{d}x$$

$$M_{ij}^{55} = \int_{x_a}^{x_b} I_{\mathrm{d}} \varphi_i \varphi_j \,\mathrm{d}x + \int_{x_a}^{x_b} \sum_{k=1}^{n_{\mathrm{D}}} I_{\mathrm{d}}^{\mathrm{D}} \varphi_i \varphi_j \Delta(x - x_{\mathrm{D}k}) \mathrm{d}x$$

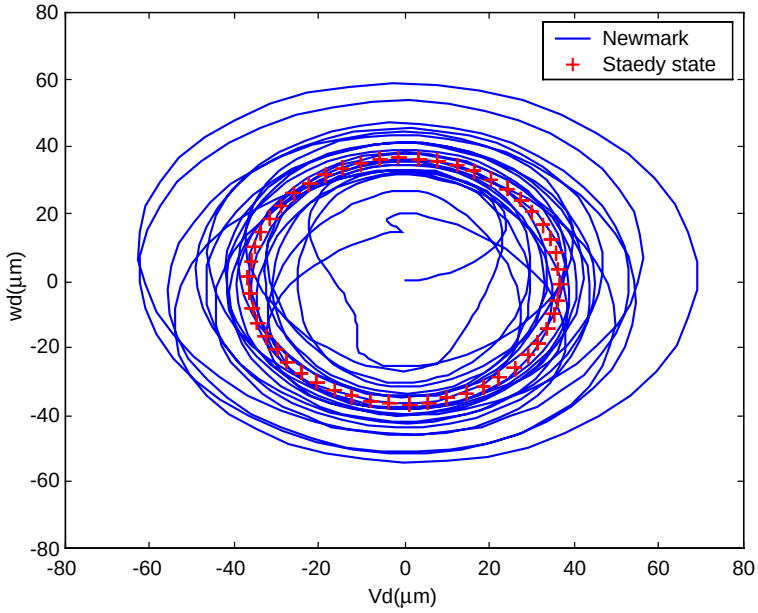

Fig. 13. The transient response of the displacement at the disk center obtained using the Newmark-β method compared with the steady-state response.

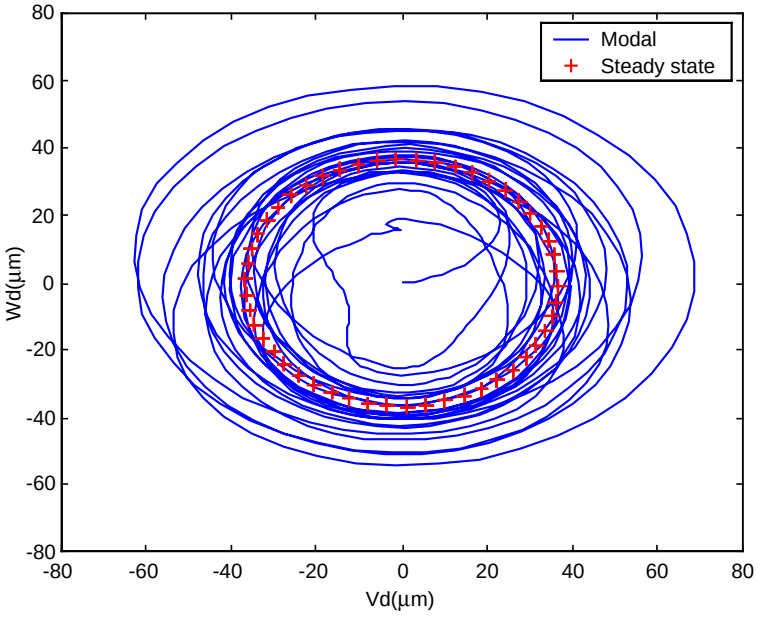

Fig. 14. The transient response of the displacement at the disk center obtained using the modal analysis method compared with the steady-state response.

$$M_{ij}^{66} = \int_{x_a}^{x_b} I_{\mathrm{p}} \varphi_i \varphi_j \,\mathrm{d}x + \int_{x_a}^{x_b} \sum_{k=1}^{n_{\mathrm{D}}} I_{\mathrm{p}}^{\mathrm{D}} \varphi_i \varphi_j \Delta(x - x_{\mathrm{D}k}) \mathrm{d}x$$

A.2. Gyroscopic matrix

$$[G^{\mathrm{e}}] = \begin{bmatrix} [0]_{3\times3} & [0]_{3\times3} & [0]_{3\times3} & [0]_{3\times3} & [0]_{3\times3} & [0]_{3\times3} \\ [0]_{3\times3} & [0]_{3\times3} & [0]_{3\times3} & [0]_{3\times3} & [0]_{3\times3} & [0]_{3\times3} \\ [0]_{3\times3} & [0]_{3\times3} & [0]_{3\times3} & [0]_{3\times3} & [0]_{3\times3} & [0]_{3\times3} \\ [0]_{3\times3} & [0]_{3\times3} & [0]_{3\times3} & [0]_{3\times3} & [G^{45}]_{3\times3} & [0]_{3\times3} \\ [0]_{3\times3} & [0]_{3\times3} & [0]_{3\times3} & [G^{54}]_{3\times3} & [0]_{3\times3} & [0]_{3\times3} \\ [0]_{3\times3} & [0]_{3\times3} & [0]_{3\times3} & [0]_{3\times3} & [0]_{3\times3} & [0]_{3\times3} \end{bmatrix}_{18\times18}$$

in which

$$G_{ij}^{45} = \int_{x_a}^{x_b} I_{\mathrm{p}} \varphi_i \varphi_j \,\mathrm{d}x + \int_{x_a}^{x_b} \sum_{k=1}^{n_{\mathrm{D}}} I_{\mathrm{p}}^{\mathrm{D}} \varphi_i \varphi_j \Delta(x - x_{\mathrm{D}k}) \mathrm{d}x$$

$$G_{ij}^{54} = \int_{x_a}^{x_b} -I_{\mathrm{p}} \varphi_i \varphi_j \,\mathrm{d}x + \int_{x_a}^{x_b} \sum_{k=1}^{n_{\mathrm{D}}} -I_{\mathrm{p}}^{\mathrm{D}} \varphi_i \varphi_j \Delta(x - x_{\mathrm{D}k}) \mathrm{d}x$$

A.3. Damping matrix of bearings

$$[C_{\mathrm{b}}^{\mathrm{e}}] = \begin{bmatrix} [0]_{3\times3} & [0]_{3\times3} & [0]_{3\times3} & [0]_{3\times3} & [0]_{3\times3} & [0]_{3\times3} \\ [0]_{3\times3} & [C^{22}]_{3\times3} & [C^{23}]_{3\times3} & [0]_{3\times3} & [0]_{3\times3} & [0]_{3\times3} \\ [0]_{3\times3} & [C^{32}]_{3\times3} & [C^{33}]_{3\times3} & [0]_{3\times3} & [0]_{3\times3} & [0]_{3\times3} \\ [0]_{3\times3} & [0]_{3\times3} & [0]_{3\times3} & [0]_{3\times3} & [0]_{3\times3} & [0]_{3\times3} \\ [0]_{3\times3} & [0]_{3\times3} & [0]_{3\times3} & [0]_{3\times3} & [0]_{3\times3} & [0]_{3\times3} \\ [0]_{3\times3} & [0]_{3\times3} & [0]_{3\times3} & [0]_{3\times3} & [0]_{3\times3} & [0]_{3\times3} \end{bmatrix}_{18\times18}$$

in which

$$C_{ij}^{22} = \int_{x_a}^{x_b} \left\{ \sum_{k=1}^{n_{\mathrm{b}}} C_{YY}^{\mathrm{b}k} \varphi_i \varphi_j \Delta(x - x_{\mathrm{b}k}) \right\} \mathrm{d}x$$

$$C_{ij}^{23} = \int_{x_a}^{x_b} \left\{ \sum_{k=1}^{n_{\mathrm{b}}} C_{YZ}^{\mathrm{b}k} \varphi_i \varphi_j \Delta(x - x_{\mathrm{b}k}) \right\} \mathrm{d}x$$

$$C_{ij}^{33} = \int_{x_a}^{x_b} \left\{ \sum_{k=1}^{n_{\mathrm{b}}} C_{ZZ}^{\mathrm{b}k} \varphi_i \varphi_j \Delta(x - x_{\mathrm{b}k}) \right\} \mathrm{d}x$$

$$C_{ij}^{32} = \int_{x_a}^{x_b} \left\{ \sum_{k=1}^{n_b} C_{ZY}^{bk} \varphi_i \varphi_j \Delta(x - x_{bk}) \right\} dx$$

A.4. Stiffness matrix

$$[K^e] = \begin{bmatrix} [K^{11}]_{3\times3} & [0]_{3\times3} & [0]_{3\times3} & [0]_{3\times3} & [0]_{3\times3} & [K^{16}]_{3\times3} \\ [0]_{3\times3} & [K^{22}]_{3\times3} & [K^{23}]_{3\times3} & [K^{24}]_{3\times3} & [K^{25}]_{3\times3} & [0]_{3\times3} \\ [0]_{3\times3} & [K^{32}]_{3\times3} & [K^{33}]_{3\times3} & [K^{34}]_{3\times3} & [K^{35}]_{3\times3} & [0]_{3\times3} \\ [0]_{3\times3} & [K^{42}]_{3\times3} & [K^{43}]_{3\times3} & [K^{44}]_{3\times3} & [K^{45}]_{3\times3} & [0]_{3\times3} \\ [0]_{3\times3} & [K^{52}]_{3\times3} & [K^{53}]_{3\times3} & [K^{54}]_{3\times3} & [K^{55}]_{3\times3} & [0]_{3\times3} \\ [K^{61}]_{3\times3} & [0]_{3\times3} & [0]_{3\times3} & [0]_{3\times3} & [0]_{3\times3} & [K^{66}]_{3\times3} \end{bmatrix}_{18\times18}$$

in which

$$K_{ij}^{11} = \int_{x_a}^{x_b} A_{11} \frac{\partial \varphi_i}{\partial x} \frac{\partial \varphi_j}{\partial x} dx$$

$$K_{ij}^{16} = \int_{x_a}^{x_b} k_s B_{16} \frac{\partial \varphi_i}{\partial x} \frac{\partial \varphi_j}{\partial x} dx$$

$$K_{ij}^{22} = \int_{x_a}^{x_b} \left\{ k_s (A_{55} + A_{66}) \frac{\partial \varphi_i}{\partial x} \frac{\partial \varphi_j}{\partial x} + \sum_{k=1}^{n_b} K_{YY}^{bk} \varphi_i \varphi_j \Delta(x - x_{bk}) \right\} dx$$

$$K_{ij}^{23} = \int_{x_a}^{x_b} \left\{ \sum_{k=1}^{n_b} K_{YZ}^{bk} \varphi_i \varphi_j \Delta(x - x_{bk}) \right\} dx$$

$$K_{ij}^{24} = \int_{x_a}^{x_b} -\frac{1}{2} k_s B_{16} \frac{\partial \varphi_i}{\partial x} \frac{\partial \varphi_j}{\partial x} dx$$

$$K_{ij}^{25} = \int_{x_a}^{x_b} -k_s (A_{55} + A_{66}) \frac{\partial \varphi_i}{\partial x} \varphi_j dx$$

$$K_{ij}^{33} = \int_{x_a}^{x_b} \left\{ (k_s (A_{55} + A_{66})) \frac{\partial \varphi_i}{\partial x} \frac{\partial \varphi_j}{\partial x} + \sum_{k=1}^{n_b} K_{ZZ}^{bk} \varphi_i \varphi_j \Delta(x - x_{bk}) \right\} dx$$

$$K_{ij}^{32} = \int_{x_a}^{x_b} \left\{ \sum_{k=1}^{n_b} K_{ZY}^{bk} \varphi_i \varphi_j \Delta(x - x_{bk}) \right\} dx$$

$$K_{ij}^{34} = \int_{x_a}^{x_b} k_s (A_{55} + A_{66}) \frac{\partial \varphi_i}{\partial x} \varphi_j dx$$

$$K_{ij}^{35} = \int_{x_a}^{x_b} -\frac{1}{2} k_s B_{16} \frac{\partial \varphi_i}{\partial x} \frac{\partial \varphi_j}{\partial x} dx$$

$$K_{ij}^{44} = \int_{x_a}^{x_b} \left\{ k_s(A_{55} + A_{66})\varphi_i\varphi_j + D_{11}\frac{\partial\varphi_i}{\partial x}\frac{\partial\varphi_j}{\partial x} \right\} \mathrm{d}x$$

$$K_{ij}^{42} = \int_{x_a}^{x_b} -\frac{1}{2}k_s B_{16}\frac{\partial\varphi_i}{\partial x}\frac{\partial\varphi_j}{\partial x}\,\mathrm{d}x$$

$$K_{ij}^{43} = \int_{x_a}^{x_b} k_s(A_{55} + A_{66})\varphi_i\frac{\partial\varphi_j}{\partial x}\,\mathrm{d}x$$

$$K_{ij}^{45} = \int_{x_a}^{x_b} \frac{1}{2}k_s B_{16}\frac{\partial\varphi_i}{\partial x}\varphi_j - \frac{1}{2}k_s B_{16}\varphi_i\frac{\partial\varphi_j}{\partial x}\,\mathrm{d}x$$

$$K_{ij}^{55} = \int_{x_a}^{x_b} \left\{ k_s(A_{55} + A_{66})\varphi_i\varphi_j + D_{11}\frac{\partial\varphi_i}{\partial x}\frac{\partial\varphi_j}{\partial x} \right\} \mathrm{d}x$$

$$K_{ij}^{52} = \int_{x_a}^{x_b} -k_s(A_{55} + A_{66})\varphi_i\frac{\partial\varphi_j}{\partial x}\,\mathrm{d}x$$

$$K_{ij}^{53} = \int_{x_a}^{x_b} -\frac{1}{2}k_s B_{16}\frac{\partial\varphi_i}{\partial x}\frac{\partial\varphi_j}{\partial x}\,\mathrm{d}x$$

$$K_{ij}^{54} = \int_{x_a}^{x_b} -\frac{1}{2}k_s B_{16}\frac{\partial\varphi_i}{\partial x}\varphi_j + \frac{1}{2}k_s B_{16}\varphi_i\frac{\partial\varphi_j}{\partial x}\,\mathrm{d}x$$

$$K_{ij}^{66} = \int_{x_a}^{x_b} k_s D_{66}\frac{\partial\varphi_i}{\partial x}\frac{\partial\varphi_j}{\partial x}\,\mathrm{d}x$$

$$K_{ij}^{61} = \int_{x_a}^{x_b} k_s B_{16}\frac{\partial\varphi_i}{\partial x}\frac{\partial\varphi_j}{\partial x}\,\mathrm{d}x$$

References

Alam, N., Asnani, N.T., 1984. Vibration and damping analysis of a multilayered cylindrical shell, part I: Theoretical analysis. AIAA Journal 22, 803–809.

Bert, C.W., 1992. The effect of bending–twisting coupling on the critical speed of a driveshafts. In: Proceedings, 6th Japan–US Conference on Composites Materials, Orlando, FL. Technomic, Lancaster, PA, pp. 29–36.

Bert, C.W., Kim, C.D., 1995. Whirling of composite-material driveshafts including bending–twisting coupling and transverse shear deformation. Journal of Vibration and Acoustics 117, 17–21.

Chang, M.-Y., Jan, J.-C., 1996. The analysis of the performance of the main spindle of the Six-Axis Tilted Bed CNC Lathe, Final Report for the Goodway Machine Corp. Ltd.

Dharmarajan, S., McCutchen Jr., H., 1973. Shear coefficients for orthotropic beams. Journal of Composite Materials 7, 530–535.

dos Reis, H.L.M., Goldman, R.B., Verstrate, P.H., 1987. Thin-walled laminated composite cylindrical tubes: Part III—Critical speed analysis. Journal of Composites Technology and Research 9, 58–62.

Faust, H., Mack, J., Spencer, B., 1984. A composite rotor shaft for the chinook. Journal of the American Helicopter Society 29, 54–58.

Fung, Y.C., 1994. A First Course in Continuum Mechanics, third ed. Prentice-Hall.

Kim, C.D., Bert, C.W., 1993. Critical speed analysis of laminated composite, hollow drive shafts. Composites Engineering 3, 633–643.

Lalanne, M., Ferraris, G., 1990. Rotordynamics Prediction in Engineering. John Wiley and Sons.

Meirovitch, L., 1990. Dynamics and Control of Structures. John Wiley and Sons.

Nelson, H.D., Mcvaugh, J.M., 1976. The dynamics of rotor-bearing systems using finite elements. Journal of Engineering for Industry, 593–600.

Nelson, H.D., Rajan, M., Chen, W.J., 1986. Parameter sensitivity in the dynamics of rotor-bearing system. Journal of Vibration, Acoustics, Stress and Reliability in Design 108, 197–205.

Ruhl, R.L., Booker, J.F., 1972. A finite element model for distributed parameter turborotor systems. Journal of Engineering for Industry (Feb.), 126–132.

Singh, S.P., Gupta, K., 1996. Composite shaft rotordynamic analysis using a layerwise theory. Journal of Sound and Vibration 191 (5), 739–756.

Song, O., Jeong, N.-H., Librescu, L., 2001. Implication of conservative and gyroscopic forces on vibration and stability of an elastically tailored rotating shaft modeled as a composite thin-walled beam. Journal of Acoustical Society of America 109 (3), 972–981.

Vinson, J.R., Sierakowski, R.L., 1986. The Behavior of Structures Composed of Composite Materials. Martinus Nijhoff Publishers, Dordrecht.

Zinberg, H., Symonds, M.F., 1970. The Development of an Advanced Composite Tail Rotor Driveshaft, Presented at the 26th Annual Forum of the American helicopter Society, Washington, DC, June.